Self-Assembled Polymer Membranes (SELFMEM)

www.selfmem.eu
www.selfmem-dissemination.org

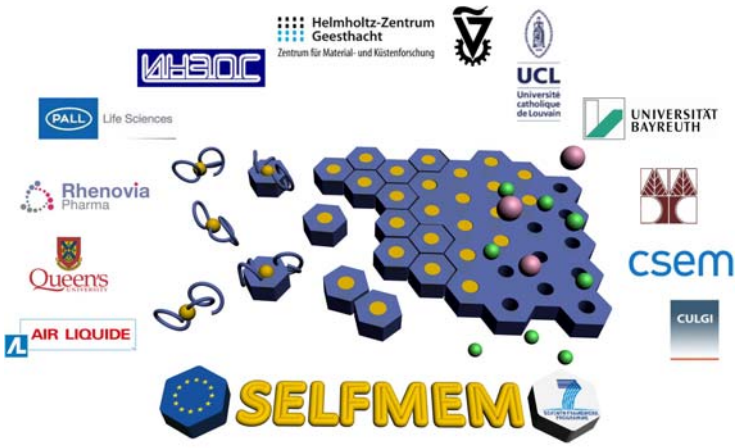

SELFMEM was organised in a number of work packages dealing with the synthesis of block copolymers, preparation and functionalization of membranes, theoretical understanding of the self-assembly during membrane formation and its simulation, and testing the suitability of the developed membranes for various applications, such as protein filtration, water purification, and gas separation.

Work Package 3: Synthesis, Characterization, and Theory of Block Copolymers

A multitude of functional diblock copolymers and ABC triblock terpolymers, derived from binary or ternary combinations of inexpensive, commercially available monomers, were synthesized using controlled polymerization techniques, including anionic polymerization, group transfer polymerization (GTP), reversible addition-fragmentation chain transfer (RAFT) polymerization and atom transfer radical polymerization (ATRP). In most cases, the combination of styrene (S) in one block and vinyl pyridine (VP) and / or ethylene oxide (EO) in the other block(s), along with the high overall polymer molecular weight, above 100 kDa and up to 600 kDa, led to phase separation on the nanoscale, resulting in spherical or cylindrical bulk morphologies which would assist in pore formation within the fabricated organic (in WP5) and inorganic (in WP6) nanoporous membranes.

Most of the copolymers prepared comprised polyS and polyVP (either the 2VP or the 4VP isomer) blocks, owing to the well-established thermodynamic incompatibility of these two polymers. These syntheses were performed using anionic polymerization, RAFT polymerization, and even combination of anionic (for the polyS block) with RAFT (for the VP block) polymerizations. The total number of synthesized polyS-poly4VP and polyS-poly2VP diblocks were 72 and 51, respectively, from which 61, 10 and one polyS-poly4VP diblocks were prepared by anionic, RAFT and anionic-RAFT polymerizations, respectively, and 20, 23 and 8 polyS-poly2VP diblocks were prepared by anionic, RAFT and anionic-RAFT polymerizations, respectively. It is noteworthy that three polyS-poly4VP diblocks

with perdeuterated styrene blocks were also synthesized using anionic polymerization. PolyS-polyEO diblock copolymers (×17) were also prepared by anionic polymerization (×15) and ATRP (×2), since the particular monomer combination was recently shown by our Consortium to exhibit sufficient incompatibility not only for microphase separation but also for successful membrane fabrication through phase inversion.

Various other diblock copolymers were prepared using anionic polymerization and the pair-wise combinations of the monomers styrene (S), methoxy di(ethylene glycol) methacrylate (DEGEMA), 2-hydroxyethyl methacrylate (HEMA), 4-(*tertiary*-butyl)styrene (4*t*BuS), 4-vinyl pyridine (4VP), 4-(trimethylsilyl)styrene (4TMSiS), and methacrylic acid (MAA). In particular, the following combinations were afforded: S-DEGEMA (×2), S-HEMA (×1), 4*t*BuS-4VP (×2), 4TMSiS-4VP (×2), and S-MAA (×1). Furthermore, anionic and RAFT polymerizations were combined to yield five diblock copolymers of S with *N*-isopropylacrylamide (NIPAAm). Another binary combination of monomers involved that of S with 2-(dimethylamino)ethyl mtehacrylate (DMAEMA), for which RAFT polymerization was used to prepare 10 linear diblock and two hyperbranched block copolymers. In a similar spirit, and using benzyl methacrylate (BzMA) instead of S (the former is the methacrylate analogue of the latter) together with DMAEMA, and ethylene glycol dimethacrylate (EGDMA) cross-linker, star (×3) and hyperbranched (×4) DMAEMA-BzMA copolymers were synthesized by GTP.

Ten ABC triblock terpolymers were also prepared using anionic polymerization. These included three S-*b*-2VP-*b*-EO, four S-*b*-2VP-*b*-(*tertiary*-butyl methacrylate) (*t*BuMA), one S-*b*-4VP-*b*-HEMA, one S-*b*-4VP-*b*-(propylene sulfide) (PSU), and one 4*t*BuS-*b*-S-*b*-4VP triblock terpolymers. Two S-*b*-EO-*b*-NIPAAm triblock terpolymers were synthesized, too, where the first two blocks were afforded by sequential anionic polymerization and the third NIPAAm block by RAFT polymerization (after the appropriate modification of a terminal hydroxyl-group already introduced during the synthesis by anionic polymerization). Some more complex symmetrical polymers were prepared by RAFT polymerization, using a bifunctional PEO-based initiator (macromolecular chain transfer agent), using one or more of S, 2VP, and methyl methacrylate (MMA). In particular, these included five ABA triblock copolymers (two based on S-EO-S, two based on 2VP-EO-2VP and one based on MMA-EO-MMA), 6 ABCBA pentablock terpolymers (two based on 2VP-S-EO-S-2VP, two based on S-2VP-EO-2VP-S, one based on S-MMA-EO-MMA-S, and one based on 2VP-MMA-EO-MMA-2VP), and two ABCDCBA heptablock quaterpolymers (one based on 2VP-S-MMA-EO-MMA-S-2VP, and one based on S-2VP-MMA-EO-MMA-2VP-S). Finally, five ABA triblock copolymers with a polysulfone mid-block and poly(*tertiary*-butyl acrylate) (P*t*BuA) end-blocks were prepared by employing condensation polymerization for the synthesis of the mid-block and ATRP for growing the end-blocks off the bromine-capped ends of the mid-block.

Another useful functionality incorporated in some of the prepared block copolymers was degradability, most notably photolability, but also thermal lability or hydrolyzability. This property can help convert the minority nanophase (cylinder or sphere) of a film to a membrane pore. Seven diblock copolymers (3 × polyEO-*b*-polyS, 1 × polyEO-*b*-poly*t*BuA, and 3 × polyS-*b*-polyMMA) whose block junction comprised a photolabile *ortho*-nitrobenzyl ester group, and one polyEO-polyS diblock copolymer with a photolabile carbamate block junction were prepared using the ATRP of S, *t*BuA or MMA, and simultaneously clicking the polyEO or polyS blocks on to two appropriately designed and synthesized ATRP initiators. Irradiating (350 nm) the resulting diblock copolymers (either in solution or as films) led to the separation of the two constituting blocks, one with a nitrosobenzaldehyde end-group (polyEO

or polyS) and the other (polyS, poly*t*BuA or polyMMA) with a carboxylic acid (case of the *ortho*-nitrobenzyl ester-based initiator) or a primary amine end-group (case of the carbamate-based initiator); note that the primary amine end-group is better amenable to chemical modification as compared to the carboxylic acid one. In a final example in this category, a polyEO-*b*-poly[(2-cinnamoyloxyethyl acrylate)-*co*-(perfluorooctyloyloxyethyl acrylate)] (PEO-*b*-PCEA-*co*-PFOctEA) diblock terpolymer was prepared by ATRP, in which the PEO block was connected to the second block again through a photolabile *ortho*-nitrobenzyl ester linkage. After casting films from this last terpolymer and vapor-annealing them, the PEO block was cleaved off by photolysis, and removed by extraction with methanol, allowing the preparation of thin films containing permeating channels. Cross-linking of the CEA units in the terpolymer film, together with the strong hydrophobic nature of the perfluorinated FOctEA units, secured the greater stability of films from this sample.

In a similar spirit, four diblocks of polyS and poly(*ortho*-nitrobenzyl acrylate) (polyNBzA) were also prepared using ATRP. In this case, photolysis can result in the removal of the polyNBzA side-groups, thus leading to the partial degradation of the second block and, therefore, again facilitating pore formation and converting the films in to membranes. Furthermore, because we determined that homopolymers based on the methacrylate analogues of 2VP and 4VP can lose their side-group in a similar fashion to polyNBzA, we prepared their diblock copolymers with polyS (as second block) using RAFT polymerization. In particular, 11 diblocks of polyS and the following pyridinyl-containing blocks were synthesized: (pyridin-2-yl)methyl methacrylate (2PyMMA, ×1), 2-(pyridin-2-yl)ethyl methacrylate (2PyEMA, ×4), 3-(pyridin-2-yl)propyl methacrylate (2PyPMA, ×3), (pyridin-3-yl)methyl methacrylate (3PyMMA, ×1), and 3-(pyridin-3-yl)propyl methacrylate (3PyPMA, ×2). From these new monomer repeating units, we determined that 2PyEMA and PyMMA are particularly attractive, because the side-group of the former can be readily and quantitatively removed under alkaline conditions, whereas that of the latter can be quantitatively photolyzed. Moreover, two diblock copolymers of polyS and polyEO, with the two blocks interconnected with ruthenium *via* terpyridine terminal groups were also prepared. Finally, the concept of degradation was also applied to homopoly(acrylic acid) (polyAA, ×2 different molecular weights) hydrogen-bonded to the polyEO block of polyS-polyEO diblocks (again ×2 different molecular weights) at four different polyAA concentrations (5, 10, 20 and 30 wt %). In this case, the complex was stable at low pH, but readily dissociated at alkaline pH; this dissociation and washing away of the polyAA was again exploited for pore formation.

WP3 also included model development for the microphase separation of block copolymer melts, in order to assist with block copolymer design.

1. A model melt of ABC triblock terpolymers, mimicking the structure of polyS-[Ru]-polyEO supramolecular macromolecules (Figure 3.1) synthesized above, was examined using the self-consistent field theory (SCFT) approach.

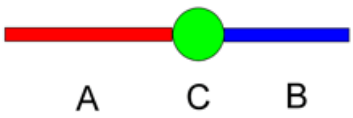

Figure 3.1: *Schematic representation of the structure of a polyS-[Ru]-polyEO supramolecular diblock copolymer, whose ruthenium block junction is to be modeled as a short third block C.*

Besides the energetic AB-incompatibility effect, which is conventionally described by the Flory-Huggins parameter χ, we also took into account the entropic immiscibility effect, i.e. a tendency for segregation of particles with different excluded volume. For this purpose, we

introduced into the free energy of the system a new asymmetric addendum, which is non-polynomial with respect to the volume fraction of "big" spheres C (block junction). We elaborated a new iteration algorithm to solve the SCFT equation with due regard for the entropic immiscibility. The preliminary calculations demonstrated that even if the energetic (χ) incompatibility is not sufficient to cause microphase separation but the excluded volume mismatch is large enough, then microphase separation could occur, in a peculiar manner, due to the entropic immiscibility: a rather strong segregation of the big spheres occurs, which quickly increases with the volume mismatch. These investigations showed that such a strong segregation would be a highly irreversible process and would, therefore, result in morphologies with many defects, thus rendering them inappropriate for membrane fabrication.

2. The peculiarities of the phase behavior of solutions of binary A_nB_m block copolymers in a solvent S were investigated within the weak segregation approach; for simplicity, we restricted ourselves to the Hildebrand approximation. The results are as follows.
i). The phase behavior of the block copolymer solutions under consideration was determined by an interplay between a tendency towards copolymer precipitation from the solvent (it leads to macrophase separation into solvent-rich and copolymer-rich phases and wins when the solvent is selective enough) and a tendency towards microphase separation (it leads to an ordering of the polymer solution into block A and block B domains intermitted with solvent S domains and wins when the solvent is more or less non-selective).
ii). The diagrams of state, which provide quantitative conditions for block copolymer to order into a 3D periodic ordered morphology or, on the contrary, to precipitate were built in the space of parameters comprising the copolymer macromolecule composition $f = N_A/(N_A + N_B)$, selectivity parameter $x = (2\delta_S - \delta_A - \delta_B)/(\delta_A - \delta_B)$ and the copolymer concentration φ_S. Unfortunately, a preliminary study of the phase diagrams within the SCFT led to the conclusion that numerical calculations are so complex that the computer power available was not sufficient to explore the whole space of parameters.

3. To understand theoretically, and as rigorously as possible, how the ion-complexation effects influence the phase diagram and morphologies arising in molten diblock copolymers under order-disorder and order-order transitions, we studied the phase behavior of a model melt of AB diblock copolymers, where all the repeating units of the A block are capable of forming thermoreversible A-A bonds. In particular, these units are supposed to bear some donor groups, which associate with each other through a bifunctional acceptor molecule (or ion) such as Cu^{2+}. Thus, the association constant dependence on the A component concentration and temperature also includes a dependence on the ion concentration.

For this purpose, we used a combination of the so-called Flory approach for the description of thermo-reversibly associating systems and the microphase separation theory, based both on the weak segregation approach and SCFT. The critical ordering point in such melts was shown to shift considerably towards smaller compositions of the A blocks capable of associating and to higher temperatures (lower values of χ). In other words, the micelles in such a melt could be reverse, i.e. their core comprises the majority component whereas the matrix is composed of the minority component. Such a behavior could be understood having in mind the fact that, after association, the elementary macromolecules in the melt are branched macromolecules (see Fig. 3.2) rather than the original linear diblock copolymer chains. Accordingly, the long-range intramolecular AB correlations, which determine the type of the resulting morphology, become to be rather different from that for the original diblock copolymer chain. A typical phase diagram is shown in Figure 3.3.

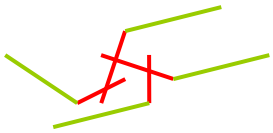

Figure 3.2: *Assocoiation of block copolymers leading to effective branched block copolymers*

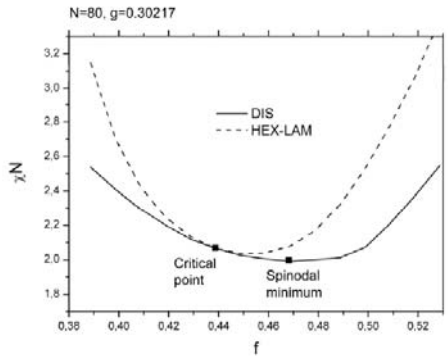

Figure 3.3: *Typical phase diagram for associating diblock copolymers (degree of polymerization N=80 and reaction constant g=0.3). Note the shift of the critical point down (from* $\chi N = 10.5$ *to* $\chi N \approx 2.1$*) and to the left (from f = 0.5 to f = 0.44).*

Work Package 4: Modeling of Membranes

In work package 4 the quantitative structure-property relationship (QSPR) modeling is applied to the self-assembly of block-copolymers to generate membranes. As WP leader Culgi was responsible for the development of a simulation protocol, INEOS provided the necessary theoretical background to the work plan and Air Liquide was responsible for the QSPR modeling. The other partners provided experimental input and feedback of the earlier versions of the simulation protocol. The final objective was to provide a simple tool to pre-screen design strategies before the actual costly experiments are carried out.

After discussion and feedback from the other partners the following parameter set and ranges were selected for the simulation study:

- Block copolymer composition: X_mY_n, m,n=50-85%
- Block copolymer mass: mass = 40 – 400 kDA,
- Weight percent block copolymer in solution: 15 – 40 %
- Solvent 1: DMF
- Solvent 2: THF
- Solvent 3: 1,4-Dioxane
- Solvent evaporation time: 2 – 15 seconds

Figure 4.1 shows the graphical user interface for the Culgi 2D dynamic density functional theory (DDFT) simulations. We choose here a field-based method to be able to fast scan the parameter phase space. Figure 4.2 shows a typical morphology obtained from the evaporation simulations of the PS-P4VP block copolymer and the corresponding image obtained from the image-processing software.

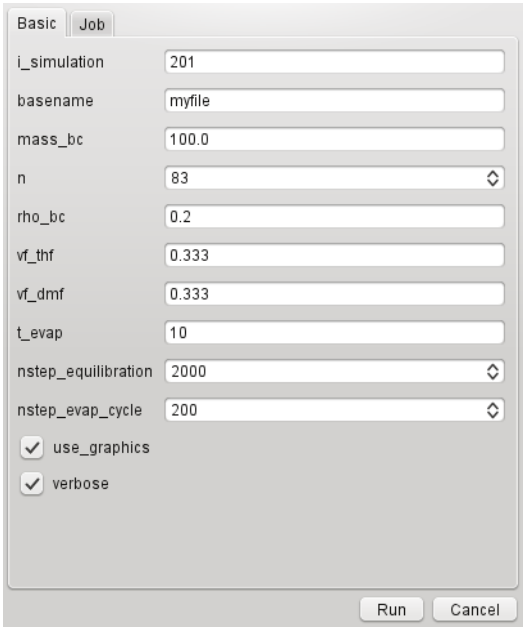

Figure 4.1: *Graphical user interface for the 2D dynamic density functional theory simulations of the membrane formation through solvent evaporation of PS-P4VP block copolymer in a THF/DMF/1,4-Dioxane solvent mixture. Volume fraction for Dioxane is computed from the values of vf_thf and vf_dmf.*

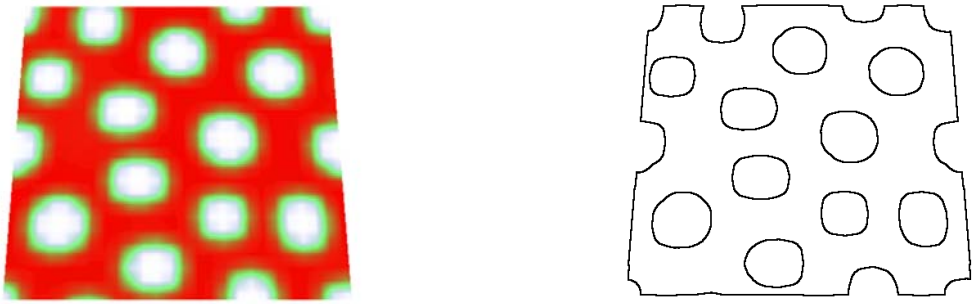

Figure 4.2: *(Right) Typical morphology of a 75 kDa PS_{75}-$P4VP_{25}$ block copolymer as obtained from the 2D-DDFT simulations. Red indicates high density, green low density and white indicates the pores. Dimensions are ~0.14 μm x ~0.14 μm. (Left) Final image obtained from the ImageJ analysis.*

The final simulation protocol consisted of the following six steps:

1. Culgi input generation (automated);
2. Run Culgi simulations (automated);
3. Analyze structure/morphology with ImageJ (automated);
4. QSPR input generation (automated);
5. Perform QSPR analysis with ModeFrontier;
6. Generate standalone, external QSPR program;

The protocol was automated using the Python scripting language. Simulations were run with the Culgi software, the image analysis was performed with ImageJ and the QSPR analysis

was done with the ModeFrontier, a software platform for numerical modeling and optimization, developed by Esteco.[1]

The following properties are computed and used as input for the QSPR analysis:

- (Average) pore size (nm)
- Standard deviation of pore size (nm)
- (Average) wall thickness (nm)
- Porosity (%)
- Feret ratio (describes pore structure)

The input parameter set (see above) led to ~ 65000 possible combinations. The 2D dynamic density functional theory simulations were run on the Linux cluster of Air Liquide at their research site at Jouy-en-Josas (France). The results were collected and used as input for the QSPR analysis, see Figure 4.3 for a typical output from this analysis.

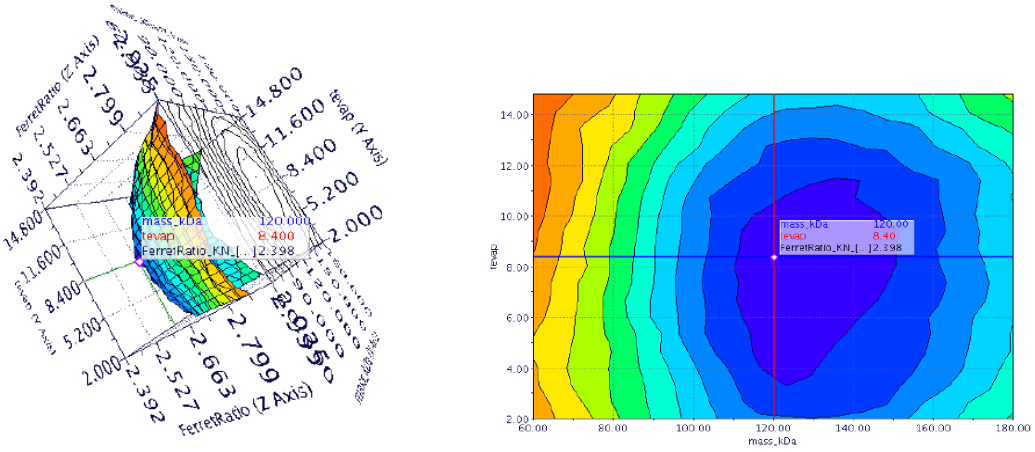

Figure 4.3: *3D (left) and 2D (right) graphical output from the ModeFrontier analysis showing a possible optimal membrane morphology in terms of the structural motifs for the variable set: block copolymer mass, evaporation rate and Feret ratio. Note that the Feret ratio is measure of the type of structural motifs found in the morphology, where a Feret ratio of 1 would indicate a perfect sphere (pore).*

All partners of the SELFMEM project got a copy of the final QSPR program as a simple Excel sheet, and so have a software tool to predict the membrane morphology before it is actually synthesized. In addition, a user can easily make a variable scan (e.g. solvent mixture or evaporation time) and get some basic idea what happens to the membrane morphology.

In summary, a robust simulation protocol has been developed for and applied to the quantitative structure-property relation (QSPR) modeling of the top layer of polystyrene poly-4-vinylpyridine (PS-4PVP) block copolymer asymmetric membranes. The protocol could, with some minor changes, be applied to any type of block copolymer, including polymers relevant to the chemical industry. Any company that would be interested in a QSPR model for their specific polymer system should be able to perform the simulation protocol in-house or, alternatively outsource it to Culgi B.V, The Netherlands. The cross sectional integral-asymmetric membrane structure is not described with this software.

[1] For more info see: www.python.org/, www.culgi.com/, rsbweb.nih.gov/ij/, and www.esteco.com/home/mode_frontier.html

Work Package 5: Block Copolymer Membranes

Block copolymer membranes were prepared via phase inversion in order to achieve high permeable and selective membranes. Different block copolymers have been used, namely polystyrene-*block*-poly(4-vinylpyridine), polystyrene-*block*-poly(2-vinylpyridine) and polystyrene-*block*-poly(ethylene oxide). High molecular weight polymers (mostly PS-*b*-P4VP and PS-*b*-P2VP) were used in order to improve the casting parameters by maximizing water permeation fluxes while a narrow pore size distribution is achieved. Moreover the use of different diblock copolymers and different volume percentages of the hydrophilic block led to the control of the pore size. The optimization of the casting conditions, upscaling of the membrane size and the reproducibility of the castings were achieved as well and the experimental parameters were given to WP4. In all cases the final membrane morphology has been characterized by scanning electron microscopy.
The study of different casting parameters and methods brought us to the conclusion that the fabrication of asymmetric block copolymer membranes with the desired morphology formed by standing cylinders is possible. Experimental prototypes of isoporous membranes from PS-*b*-P4VP and PS-*b*-P2VP have been elaborated for WP7 and WP8. The formation of such membranes is a sensitive process strongly dependent on molecular, solution and processing parameters. The solvents used for the solution preparation of PS-*b*-P4VP block copolymer membranes (Figure 5.1A) were always DMF/THF, while different polymer concentrations were used. The precipitatant was in all cases water. For the PS-*b*-P2VP block copolymer membranes the best conditions were obtained with a concentration of approx. 20wt% colymer solution in a THF/DMF mixture, which was cast with a doctor blade with a gap of 200μm. After 30s the membranes were immersed into a water bath which induced phase separation. For optimizing the formation of an integral asymmetric membrane from PS-*b*-P2VP, the solvent system and the temperature of the immersion bath were varied. The same block copolymer was dissolved in a ternary solvent mixture containing DMF/THF/dioxane (Figure 5.1B).

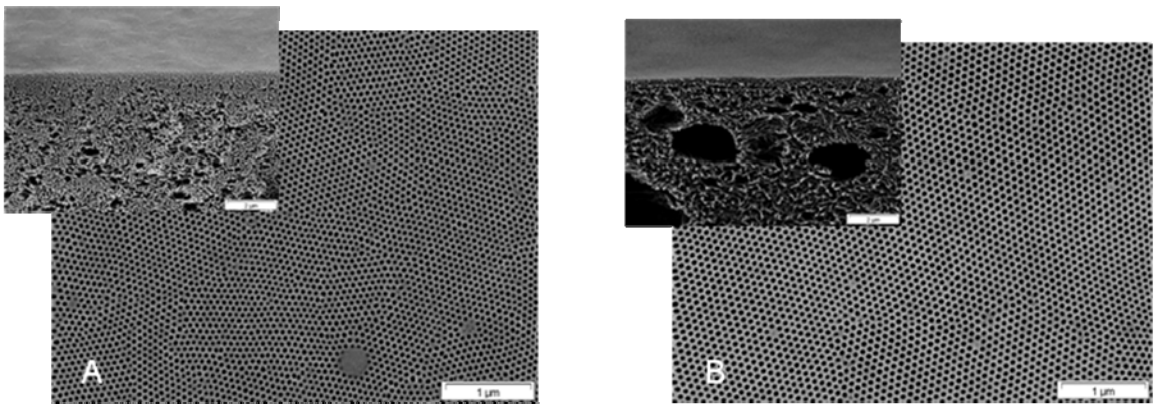

Figure 5.1: *(A) PS-b-P4VP phase inversion membrane, (B) PS-b-P2VP phase inversion membrane*

Although the reproducibility of the membranes in small scale has been extensively tested, the upscaling to bigger sizes has shown to increase the number of defects on the surface of the membrane. Therefore, a homemade casting machine (Figure 5.2) that reproduces the casting technique used in the laboratory was constructed.

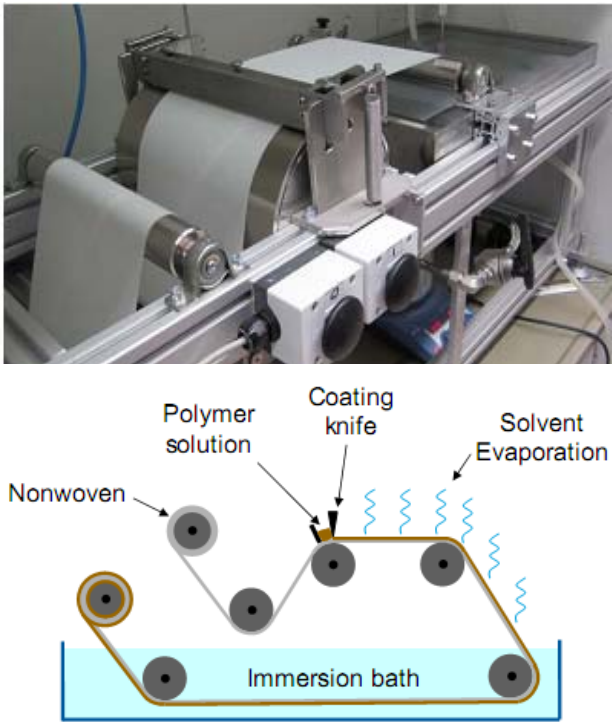

Figure 2: *Laboratory sized casting machine and the schematic representation of the operation principle.*

PS-*b*-PEO membranes were developed due to the special properties of PEO, non-ionic amphiphilic block copolymers comprising PEO are not only of scientific interest but also in terms of industrial applications. A combination of solution casting and solvent – non-solvent exchange has been applied to generate asymmetric composite membranes with highly ordered hexagonally packed cylinders with perpendicular orientation. These membranes were prepared on a nonwoven support. The development is based on the determination of the solution and precipitation behavior of PS-*b*-PEO. The best membrane structure was obtained for a ternary solvent system of DMF/THF/MeCN, from a 20 wt% polymer solution with a doctor blade height of 200 µm. After evaporating for 50s the film was dipped into the non-solvent bath (diethylether).

Within the investigation of diblock copolymer/homopolymer mixtures with non-covalent interactions (e.g. hydrogen bonds) complexes mixtures have been prepared by mixing PS-b-PEO copolymers to poly(acrylic acid) (PAA) homopolymers in variable amounts in N,N-dimethylformamide (DMF). Solutions with different concentrations have been characterized by light scattering. The formation of non-aggregated soluble PS-b-PEO/PAA complex has been confirmed. No pre-formed structures have been detected. All thin films produced have been characterized by tapping-mode AFM. The porosity has been created by washing the films with basic water. This results in the breaking of the hydrogen-bonded complexes and in the release of the ionized PAA chains in solution.

Diblock copolymers with UV-photocleavable units have been prepared: EO_{22}-hv-S_{78}[23], $S_{63}(NBA_{33}AA_4)$[39], $S_{88}(NBA_{10}AA_2)$[38], $S_{76}(NBA_{23}AA_1)$[57],$S_{82}(NBA_{16}AA_2)$[73]. Lower case numbers correspond to the weight percentage of the respective block, upper case numbers indicate the total molecular weight in kg/mol. Solutions with different concentrations were characterized by light scattering. No aggregation has been detected in the solvent used for thin film preparation (DMF). The ability of these copolymers to cleave under well-defined

conditions in solution and in the bulk has been demonstrated. Thin films have been prepared from these photocleavable block copolymers. The formation of the desired cylindrical morphology has been observed in all cases. However, solvent annealing is needed to obtain perpendicularly oriented cylinders. All these thin films have been characterized by tapping-mode AFM. Porosity has been created by exposing the films to UV-irradiation and washing off the cleaved PEO.

Additionally, a poly(ethylene oxide)-*block*-poly(2-cinnamoyloxyethyl methacrylate) or PEO-*b*-PCEMA sample has also been prepared. This diblock copolymer had a photo-cleavable group at the block junction. The block segregation pattern in thin films has been examined by atomic force microscopy. Under appropriate solvent vapor annealing conditions, the PEO cylinders were brought to a standing orientation. After photolysis, the PEO block was cleft from the PCEMA matrix. Extraction with methanol allowed preparing thin films containing permeating channels.

Hexagonal pore formation was achieved from a photocleavable PEO-h_n-PS from a spin coated solution in C_6H_6 and the annealing of these films in C_6H_6 vapours (Figure 5.3). The blending of different amounts of PS-SO_3H and PEO–$N(CH_3)_2$ and different molecular weights could lead to the control of the pore size. Molecules can be grafted inside the pores and further detached by photoirradiation via a photosensitive ester bond.

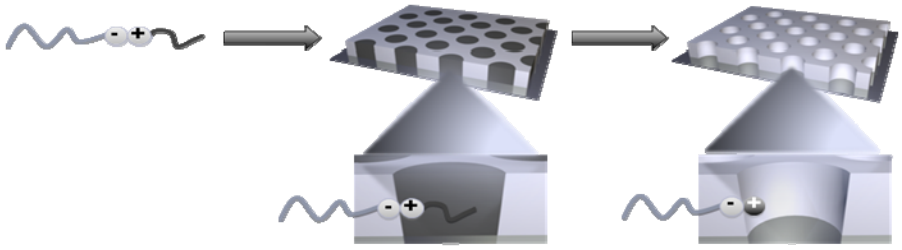

Figure 5.3: *Membranes from block copolymers with ionic junctions.*

A preliminary theoretical study of the phase behaviour of a diblock copolymer in a solvent, within the weak segregation regime, was carried out, focusing on competition between microphase separation in the three-component system AB-diblock + solvent and precipitation of the AB-diblock from solution.

Simultaneously, it was shown both analytically and via Monte-Carlo simulation that under ordering of block copolymer melts the solvent adsorbs to the domain interfaces. Thus, the geometry of the solvent fluxes is to resemble that of BCP. In the case the evaporative dissipative structures are commensurable with the supercrystal BCP morphologies one can expect that a positive feedback between the well conducting morphologies and fast evaporation occurs. Investigation of the influence of the convection on the morphologies formed could not be finished yet.

As a contribution to understand the structure of the BCP solutions of PS-*b*-P4VP during solvent evaporation, within the random phase approximation (RPA), the small-angle scattering from the Gaussian block copolymer chains in a mixed solvent taking into account different selectivities of the solvent components with respect to polystyrene and poly(4-vinylpyridine), was calculated. The results from this study strongly support the view that the

structure formation proceeds via intermediate micelle formation rather than through continuous segregation of the strongly overlapping BCP chains.

The behavior of linear diblock copolymers in solution has been investigated by dynamic light scattering experiments carried out in different solvents. It was found that the hydrodynamic diameters are higher in toluene, a selective solvent, than in DMF, a non-selective one, as expected. For the P4VP-bearing diblocks, some of the diameters are too high, a manifestation of extensive aggregation, also visible by the eye.

In the framework of WP5, the self-assembly in solution of selected block copolymers was also studied. Films formed by the copolymers were characterized with room-temperature transmission electron microscopy (TEM) and with high-resolution scanning electron microscopy (HR-SEM). To follow the structure formation process during membrane casting, the bulk morphologies in solutions of the copolymer $S_{78}4VP_{22}^{153}$, of different compositions: 20% copolymer in DHF/THF (different ratios, with and without addition of 0.25% H_2O) were studied. By this set of samples we simulated the fast evaporation of THF during solution casting, as the membrane is formed.
A focused study on the location of each block of the copolymer in the micelles formed in solution, and the effect of water addition to the system was conducted. A combination of two complementary methods was used: SANS and cryo-TEM. 5% block copolymer solutions with and without addition of small amounts of water were characterized. The comparison of the SANS curves indicates that the micellar structure is due to P4VP, and not PS, meaning that the micelles core is made of the P4VP blocks, while their shell is composed of PS blocks as a semi-dilute polymer solution in DMF.
To complement the SANS results with direct imaging, cryo-TEM specimens were prepared of similar solutions proving the presence of spherical micelles in this solution, in agreement with the SANS results (Figure 5.4).

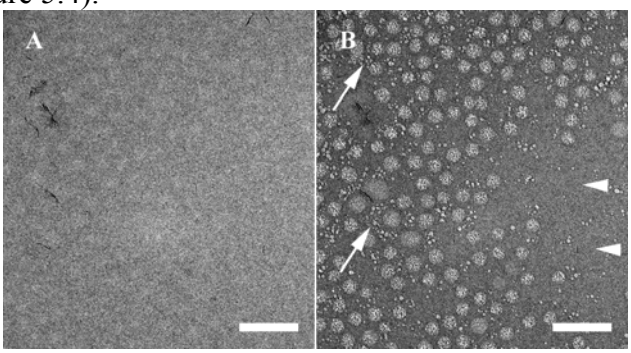

Figure 5.4: *Cryo-TEM of 5% PS_{73}-b-$P4VP_{27}$, 310 kg/mol in DMF, after different electron exposures: A. 2 $e^-/Å^2$; B. 6 $e^-/Å^2$. Arrows and arrowheads, point at differences between radiation damage in the solvent around micelles, and far from micelles, respectively. Bars correspond to 200 nm.*

SAXS experiments were also conducted by a new apparatus was designed to investigate the film formation process in situ by using synchrotron small-angle x-ray scattering. The apparatus is shown in Figure 5.5. It consists of a motor that draws a thin film support (TESA) along a doctor blade which is used to cast a film of well-defined thickness. It allows to individually adjusting the casting velocity and evaporation time until water is added via an inkjet print head. During the film formation process the scattering patterns are collected in-situ in time-frames down to seconds using state-of-the art fast read-out area detectors.

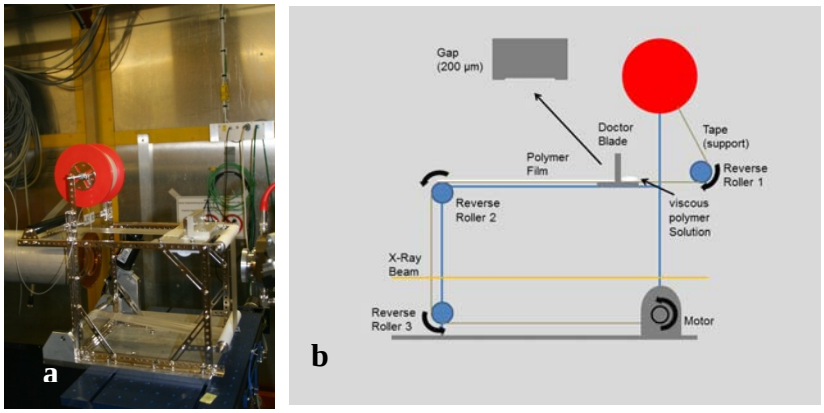

Figure 5.5: *Image (a) and Schematic drawing (b) of an automatic film casting apparatus using tape as support for the polymer-film. The synchrotron-beam meets the support and the sample at a fixed spot. Thus variation of the tape-velocity corresponds to different evaporation times on the point of measurement.*

From the analysis of these results 4 stages of structural development clearly arise:

1. Featureless scattering pattern indicating a homogeneous solution (0 - 30 sec),
2. Phase separation, presumingly into spherical micelles (35 – 55 sec), indicated by a well-defined Debye-Scherrer ring,
3. Phase inversion into a pore structure indicated by the movement (and broadening) of the Debye-Scherrer ring to lower q-values

Further phase separation indicated by the increasing scattering intensity into the final structure of the membrane.

A range of membranes was supplied to an industrial partner to be evaluated against application targets. Where the size of the membrane sheet allowed, testings were made to further study their physical properties. Pore size measurements made *via* porometry showed that at mean flow there is good correlation with those determined by SEM. Experiments performed using dyes to look at the charge of the membrane revealed that those formed from PS-*b*-P4VP possessed a positive charge, whilst those from PS-*b*-P2VP had no overall charge. The presence of a charge is interesting as it could be a contributing factor to the retention of proteins and other species.

Mechanical strength measurements showed that, in general, membranes with polymers of higher molecular weights gave greater elongation and required a higher force to break than the support itself.
Water flux and fractional filtration experiments were performed in dead-end mode using a home-made testing device at transmembrane pressures up to 2.2 bars at room temperature. These studies were conducted employing demineralized water with an electrical conductivity of ~0.055 µS cm^{-1}.

Water flow rates taken within 1 minute after the start of the experiment (initial water flow) showed that the majority of the membranes have greater flow rates than 1000 $Lm^{-2}h^{-1}bar^{-1}$. In most of the cases the average flux after 1 h of measurements in the case of PS-*b*-P4VP and PS-*b*-P2VP block copolymer membranes was dropping about 30% The highest measured flux value was for basic pH. By decreasing the pH, P2VP or P4VP are protonated and the pore size becomes smaller. Thereby the water flux goes down and at pH values around 3 the pores are almost closed, leading to minimized flux. The tuning of the pores is reversible, since the hydrophilic block can be deprotonated again; and the water flux increases again. This is

believed to be due the swelling of the hydrophilic block which reduces the pore diameter, and fouling of the surface.

In the case of the PS-*b*-PEO water flux measurements were also performed. Similarly to the above mentioned membranes at early stages of flux measurements is rather high (> 1000 L m^{-2} h^{-1} bar^{-1}). This proves the open pores generated during the membrane preparation Due to the swelling of the PEO block the flux reduces significantly within a short time. Attempts to recover the flux by reopening the pores were not successful.

Work Package 6: Nanoporous Silicon Membranes

The goal of this WP was to study and optimize the various steps leading to the fabrication of free-standing nanoporous silicon-based membranes (NSiMs). This included the formation of block copolymer thin films onto silicon substrates, the creation of nanopores of well-controlled dimensions and the release of the final free-standing membranes. The main objective was to demonstrate the process manufacturability of NSiMs at a large scale. Extensive membrane characterization was conducted at each step using AFM, TEM, HR-SEM and SAXS. The mechanical properties of the produced membranes were also determined. This work was also supported by a general theoretical study of block copolymer morphologies in thin films. Silicon membranes produced in WP6 were functionalized in WP7 and their performances evaluated in WP8.

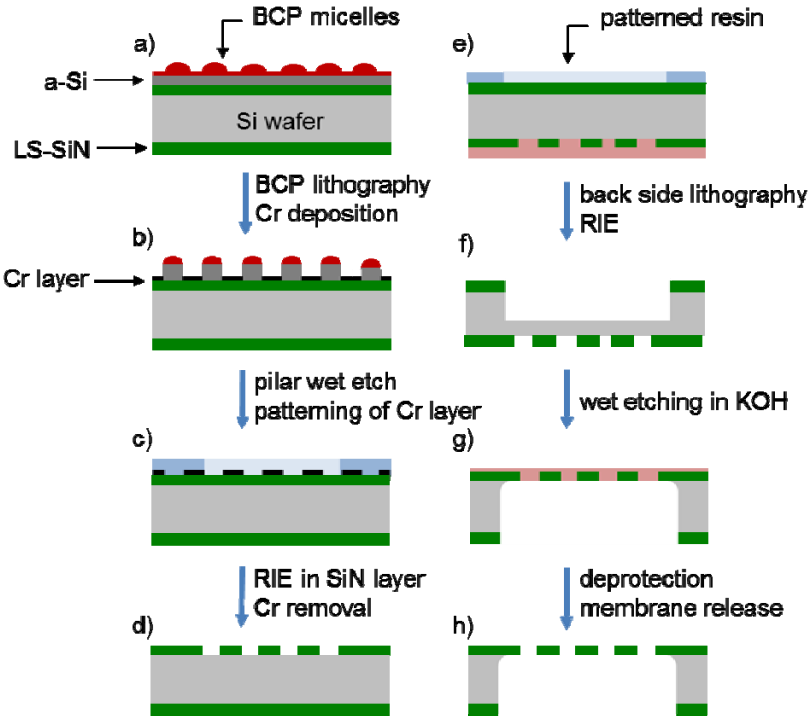

Figure 6.1: *Schematic process flow of the fabrication of ultrathin NSiMs at wafer scale.*

In a first part of this project, the self-assembling properties of di- and triblock copolymers of various natures, compositions and molecular weights have been evaluated in order to identify suitable polymer template candidates for the membrane fabrication. The work included the screening of PS-b-P2VP, PS-b-P4VP, PS-b-PAA, PS-b-PEO and PS-b-PI-b-PMMA copolymers, all produced in WP3 using anionic, ATRP or RAFT polymerization techniques.

Finally, we selected a PS-b-P2VP copolymer (74-200 kg.mol^{-1}, anionic polymerization) forming narrow size distributed spherical micelles in m-xylene, and optimized the deposition conditions (concentration, temperature, humidity, spin-coating speed) in order to produce ordered arrays of micelles on 4 in. silicon wafers in a highly reproducible manner. The micelles exhibited the following dimensions: diameter: 90 nm, height: 50 nm, density: 40/µm^2.

Then, the nanopores were produced in silicon nitride thin films by using block copolymer micelles as etching mask. Several strategies were followed in order to ensure a proper transfer of micelle topography in silicon surfaces. They included the use of intermediate metal layer deposited on the micelles, followed by a direct lift off process. This latter approach was difficult to up-scale with a good repeatability and led to incomplete removal of the micelles. An alternative method, consisting of first transferring the micelles on an amorphous silicon layer before metal evaporation allowed us to solve this issue and to produce high quality nanoporous Si and SiN layers with the targeted pore size. The schematic process flow used for the fabrication of ultrathin NSiMs at wafer scale is shown in Fig. 6.1.

During the course of the project, NSiMs were typically produced at a yield superior to 90 %. Figure 6.2 shows a 4 inch silicon wafer holding 160 pre-patterned silicon chips, each one carrying single or multiple 100 nm thick free-standing NSiMs with lateral dimensions varying from 0.5 x 0.5 mm up to 2.4 x 2.4 mm. The porous membrane is surrounded by a plain SiN frame, which is produced by using a second photomask having slightly larger openings than the one used to pattern the front side. The role of this frame is to reinforce the membrane stability by minimizing the stress distribution in the free-standing SiN film. At a higher magnification, SEM reveals that the nanopores perfectly reflect the initial arrangement of the parent BCP micelles, with a density of ~4.10^9 pores/cm^2, corresponding to a void fraction of about 0.2.

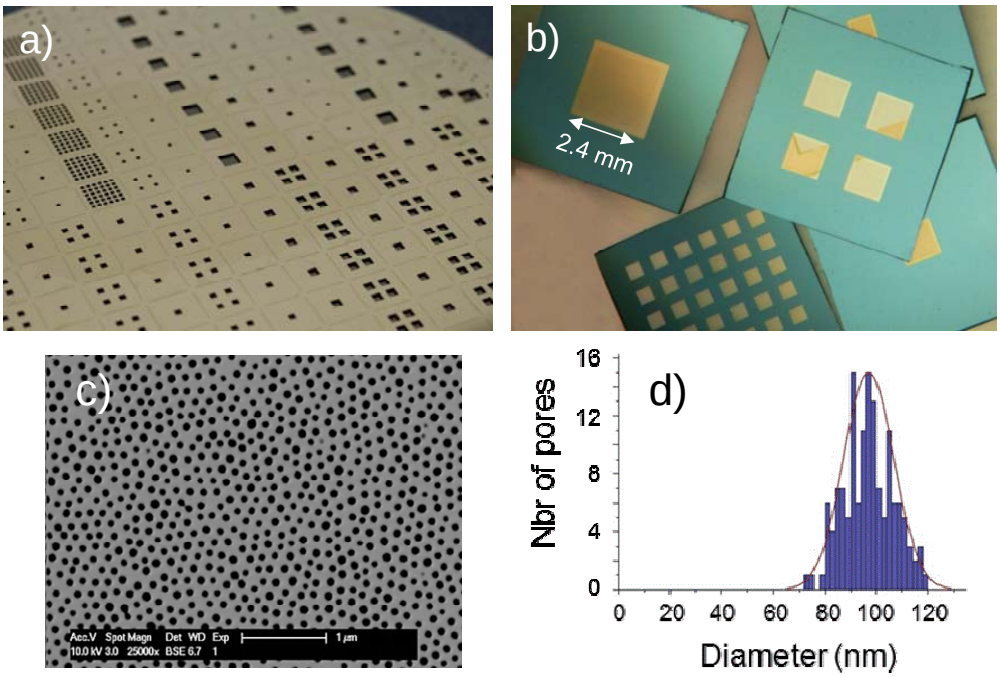

Figure 6.2: *100 nm thick free-standing NSiMs produced at wafer scale. a) Back side of a 4 inch silicon wafer showing the size of the membrane openings ranging from 0.5 x 0.5 mm up to 2 x 2 mm. b) Individual 6 x 6 mm silicon chips carrying either single or multiple free-standing NSiMs. The chips can be cleaved manually by applying a slight pressure on the wafer. c) SEM picture of the 95 nm nanopores. The scale bar is 1 µm. d) distribution of pore diameters.*

This matching implies that the size and density of the nanopores can be adjusted, to a certain extent, by simply varying the spatial dimensions of the templating micellar film. The pore size distribution shows a slight shift compared to the initial micelle sizes, with a mean nanopore diameter of about 95 nm. This is assigned to the lateral etching of SiN walls during RIE causing a slight enlargement of the nanopores. Besides block copolymers, nanosphere lithography was also implemented to standard microfabrication techniques for the fabrication of NSiMs having pore diameters above 100 nm (results not shown here). Using this technique, 100 nm and 200 nm thick free-standing NSiMs were produced with an average pore size of 250 nm and overall porosity of 15-20%.

One key property of filtration membranes developed in WP6 is their ability to withstand differential pressures without apparition of cracks in the porous layer, which can then alter their performances. Indeed, the mechanical stability defines to a large extend their possible integration in pressure-driven devices, and subsequent domains of applicability. Here, we used the bulge method to study the mechanical strength of NSiMs and conducted destructive tests to determine the range of operating pressures. Fig. 3 shows the typical loading and unloading pressure-deflection curves obtained for a 100 nm thick (800/600) membrane. As usually observed for thin SiN films, the loading curves exhibit a non-linear behavior with a fast deformation at low differential pressures. A first cycle of pressure loading (until $\Delta P = 230$ mbar)/unloading shows that the two curves superpose with almost no hysteresis. This elastic behavior was confirmed for three loading/unloading cycles conducted on the same membrane (results not shown). In all cases, we observed that the membrane returned to its initial state without residual deformation or detectable damages to the nanoporous layer. The image inserts in Fig. 6.3 shows the way the membrane deforms when ΔP increases. The maximum bulge height is always kept below 27 µm, corresponding to a membrane deformation of less than 4 %. Moreover, we can clearly distinguish an accumulation of stress at the four membrane corners just before reaching the burst pressure at about 400 mbar. For demanding applications, the mechanical strength of NSiMs may be improved by either adjusting the membrane geometry/dimension, increasing the thickness of the porous SiN layer or adding supporting structures. For instance, preliminary results indicate that 200 nm thick NSiMs of slightly smaller porous area can withstand more than 1 bar differential pressure.

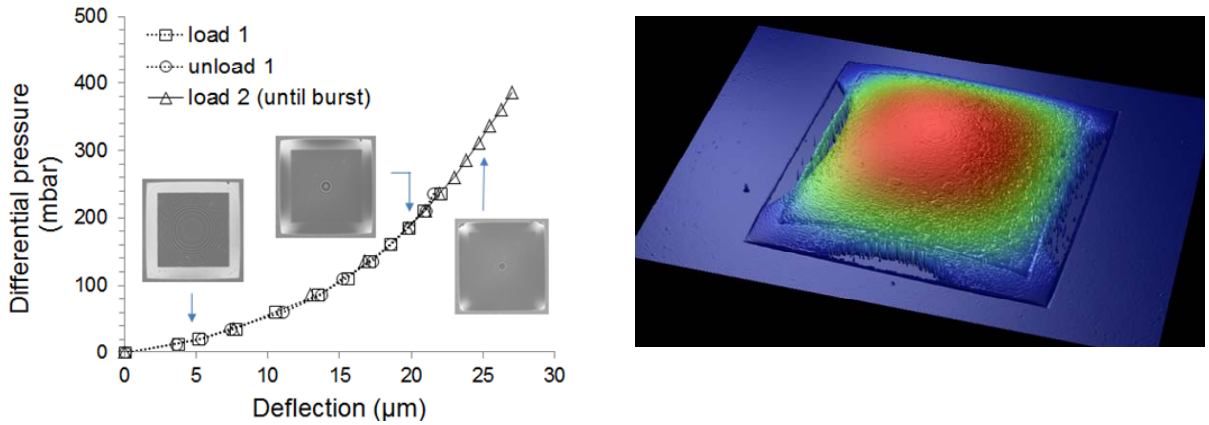

Figure 6.3: *(left) Pressure-deflection loading/unloading curves for a (800/600) NSiM. Optical images showing the membrane deformation were taken by a CCD camera at various pressures (20, 180 and 340 mbar). (right) Reconstructed images showing the deflection a free-standing NSiM when exposed to a differential pressure of 100 mbar*

A significant part of the work was also dedicated to the theoretical study of block copolymer morphologies in thin films. This task supported the experimental work by providing

theoretical insights for block copolymer self-assembly. The main concern of the theoretical study has been the new tetrapod network morphology possessing the symmetry of the diamond phase D (space group No 227). The importance of this morphology is due to the fact that it seems to possess more favorable permeability properties as compared to the lamellar and cylindrical morphologies. The phase is found to be stable in the symmetric linear ternary ABC block copolymers with the middle block long enough and non-selective with respect to the side blocks as well as in ABC-like two-scale AB block copolymers. The stability conditions for the morphology both in bulk and in thin films (membranes) are calculated within the weak segregation theory and self-consistent field theory. The wetting of the substrate along a lamellar pattern is shown to stabilize the D phase in films (Fig. 6.4).

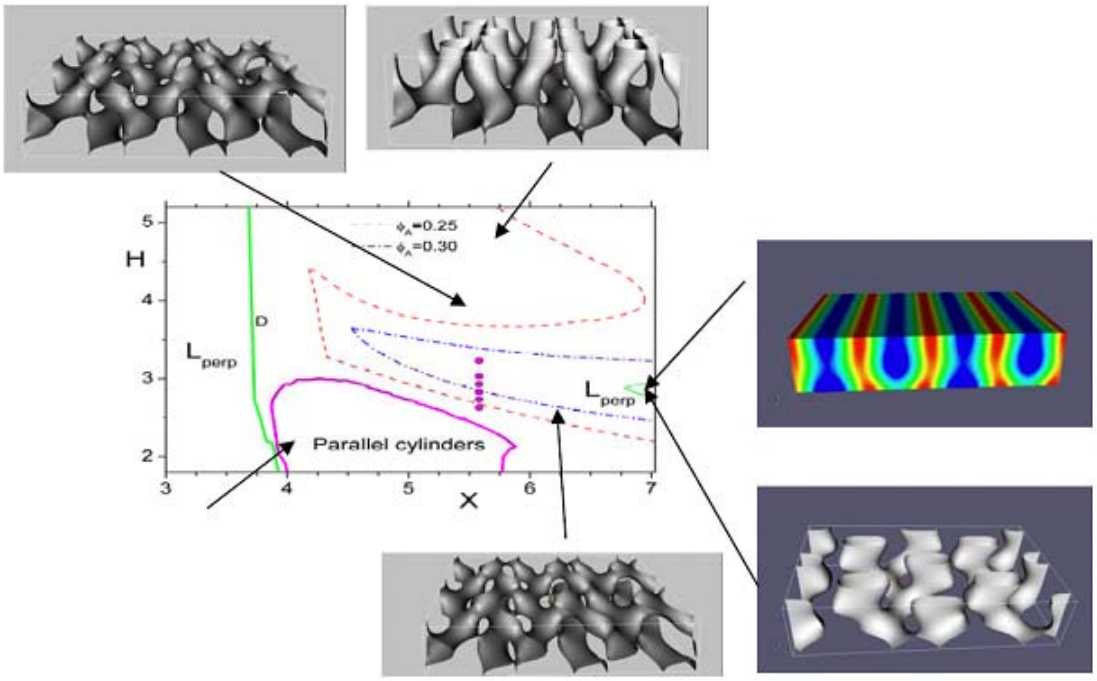

Figure 6.4: *The phase diagram of thin films of the linear ternary ABC block copolymers. The film width H and the lamellar adsorbing pattern on the walls is measured in the units of the whole chain gyration radius. The typical morphologies equilibrium in various points of the phase diagram are also shown*

In summary, the work conducted in WP6 allowed us to develop a robust and flexible process based on block polymer self-assembly for manufacturing highly porous free-standing NSiMs at wafer scale. Since the nanopores originate from the etching of micellar templates of tunable sizes and surface arrangements, the final membrane specifications can be tailored to the desired values with only minor adaptations of the process. Hence, this approach represents a valuable alternative to more sophisticated patterning techniques, such as nano-imprint, e-beam or interference lithography, for producing ultrathin silicon-based membranes with tunable pore diameters in the ultra and microfiltration range.

Work Package 7: Post-Functionalization of Membranes

In this work package, the membranes prepared in WP5 and WP6 were post-functionalized with various types of molecules (dyes, organic molecules, stimuli-responsive polymer segments, biomolecules) in order to impart new and unprecedented functionalities to the

membranes. This will significantly broaden the scope of application of the accordingly prepared membranes. For example, in addition to size selectivity, membranes with specific affinity to targeted molecules can be obtained. Three main types of post-modified membranes have been obtained in WP7 during the project: membranes with well-defined chemical functionalities inside the pores obtained from cleavable polymers or polymer complexes (i), post-functionalized pH and thermo-responsive asymmetric membranes (ii) and silicon-based membranes functionalized by (reactive) polymers (iii). In the following, the main achievements obtained on these three families will be shortly described.

7.1. Membranes with well-defined chemical functionalities inside the pores obtained from cleavable polymers or polymer complexes

7.1.1.Membranes with functionalized nanopores from block copolymer/homopolymer complexes (UCL)

Polystyrene-*block*-poly(acrylic acid) (PS-PAA) block copolymers have been mixed to poly(ethylene oxide) (PEO) homopolymers in variable amounts. PS-PEO copolymers have been also mixed with PAA homopolymers. Those mixtures have been spin-coated on silicon wafers to obtain thin films. The formation of the desired cylindrical morphology has been observed in all cases. Moreover the hydrogen-bonded PAA/PEO complexes support a perpendicular orientation of the cylinders in the film. Porosity has been created by washing the films with basic water. This results in the breaking of the hydrogen-bonded complexes and in the release of the PEO chains in case of PS-PAA/PEO blends and of the PAA chains in case of the PS-PEO/PAA blends. This results in a PS matrix with hairy pores covered by PAA chains (see Fig. 7.1, left) in case of PS-PAA/PEO blends or in a PS matrix with hairy PEO pores in case of the PS-PEO/PAA blends. The diameter of the pores as well as the inter-cylindrical pore distance was found to increase with the amount of added PEO in the PS-PAA/PEO blend. Moreover, adding a too large amount of PEO leads to a phase transition towards a lamellar morphology.

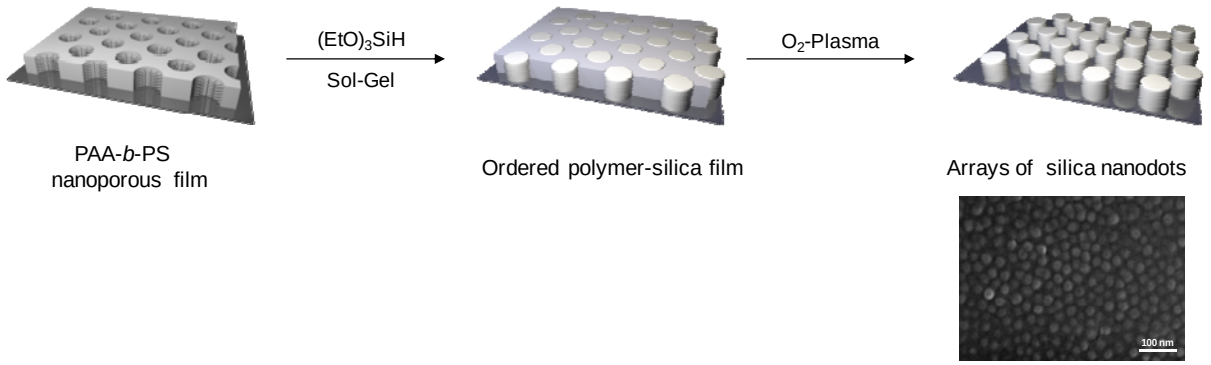

Figure 7.1: *Schematic representation of the hairy pores obtained after PEO removal in membranes formed by PS-PAA/PEO blends (on the right) and formation of an array of silica nanodots templated in such a membrane (left).*

A fluorescent dye (pyrenyl diazomethane or PDAM) has been covalently grafted inside the pores of the membranes via the formation of an ester bond between the carboxylic acid groups covering the pores and PDAM. In a last step, post-functionalization of those membranes has been achieved by performing sol-gel chemistry inside the pores. To this aim, triethoxysilane has been condensed in silica nanoparticles. Fig. 7.1 shows that silica nanoparticles templated by the porous membranes have been obtained.

7.1.2. Membranes with functionalized nanopores obtained from photocleavable block copolymers (UCL)

Photocleavable block copolymers bearing either a photocleavable group at the block junction or photocleavable side-chains have been synthesized. The photocleavable moieties are ortho-nitrobenzyl derivatives. After photocleavage, those block copolymers lead to membranes with chemical functions at the pore walls for the block copolymers with a photocleavable group at the block junction while it leads to membranes with hairy nanopores for block copolymers with photocleavable side-chains. Thin films have been prepared from these photocleavable block copolymers. The formation of the desired cylindrical morphology has been observed in all cases after solvent annealing. Porosity has been created by exposing the films to UV-irradiation and washing the cleaved PEO blocks. FTIR spectroscopy and UV-vis spectroscopy have been used to ascertain the cleavage of the ortho-nitrobenzyl moieties and the release of the PEO blocks in solution. The porosity has also been evidenced by transmission and scanning electron microscopies.

The possibility to use the reactive groups left on the pore walls after photocleavage and PEO removal has been demonstrated by chemical grafting of a fluorescent derivative. Moreover, the grafted molecules can be further detached by irradiating the system at 350 nm. The use of UV-light to break the photocleavable junctions allows the use of a photolithographic mask and the formation of patterned membranes with porosity selectively created in the irradiated areas.

Two families of ortho-nitrobenzyl derivatives have been utilized, namely orthonitrobenzyl esters and ortho-nitrobenzyl carbamates, leaving after photocleavage carboxylic acids and primary amines on the pore walls, respectively. Fig. 7.2 shows the chemical structure of a photocleavable block copolymer with an orthonitrobenzylcarbamate at the block junction. The amino groups generated after irradiation further allow post-functionalization of the accordingly formed membranes by fluorescent dyes with a peptidic-like coupling (Fig. 7.2). Furthermore, the patterning of the membranes via irradiation through a lithographic mask is also possible (Fig. 7.2).

7.1.3. Membranes with functionalized nanopores obtained from ionically connected block copolymers (UCL)

Membranes have been also prepared from ionically connected diblock copolymers. Those copolymers have been prepared by mixing a sulfonic acid terminated PS to a dimethylamino-ended PEO. It has been demonstrated that proton transfer occurs from the sulfonic acid to the dimethylamino group resulting in the formation of an ion pair and hence, in an ionically connected PS-PEO block copolymer. After self-assembly of those block copolymers in a thin film with an array of PEO cylinders oriented perpendicularly to the films surface, the PEO blocks have been extracted by washing with methanol. This leaves a PS membrane bearing sulfonate groups on the pore walls. The post-functionalization of those membranes has been demonstrated by grafting through ionic interaction a mutually interacting fluorescent probe (Rhodamine 6G). On the other hand, a fluorescent molecule (Coumarin 343) with no complementary functional group was not retained on the membranes demonstrating the selectivity of our approach.

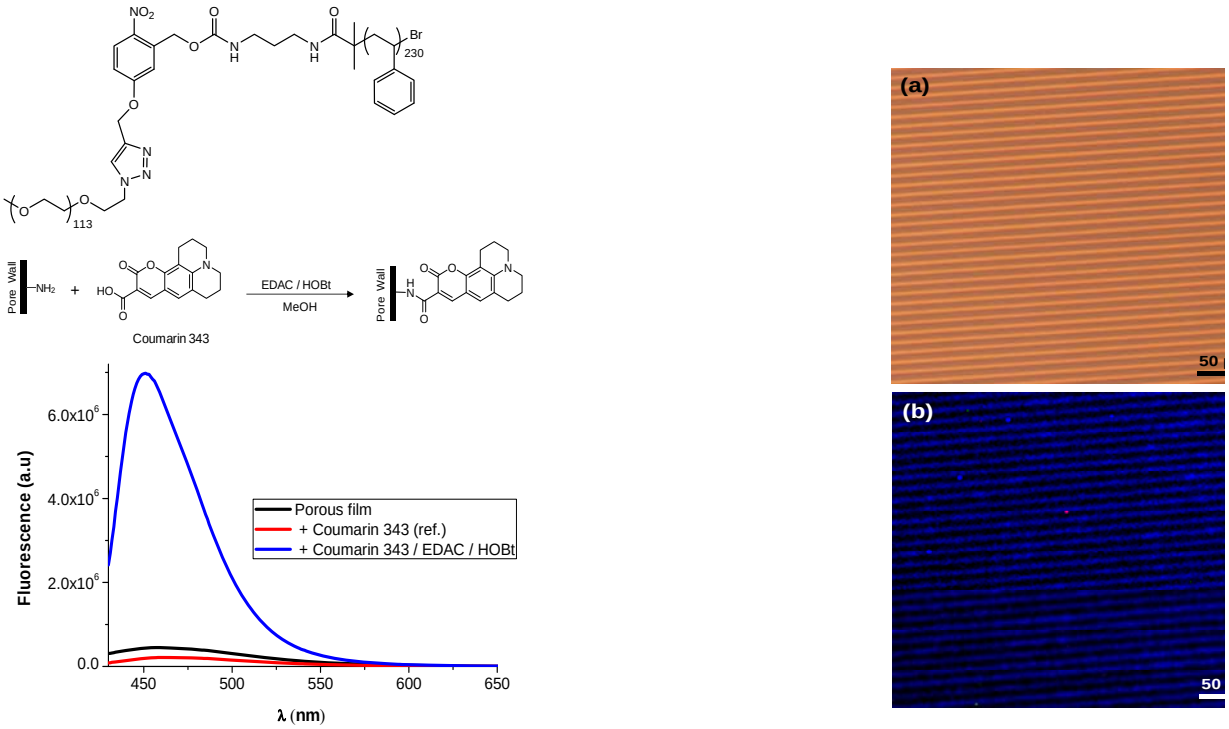

Figure 7.2: *Patterning of membranes based on a photocleavable PS-h*ν*-PEO copolymer with an ortho-nitrobenzyl carbamate junction (chemical structure on top). Post-functionalization of the pore walls by fluorescent Coumarin 343 via peptidic coupling (EDAC: 1-ethyl-3-(3-dimethylaminopropyl) carbodiimide; HOBt: hydroxybenzotriazole) and fluorescence spectra of the accordingly functionalized membrane (left). Optical microscopic image of the used mask (a). Fluorescence microscopic image of the membrane after the grafting of the blue fluorescent dyes selectively in the patterned areas (b) (right).*

7.1.4. Membranes with functionalized nanopores obtained from metallo-supramolecular block copolymers (UCL)

Block copolymers containing a metal-ligand cleavable junction were investigated (Fig. 7.3). Those systems are based on a PS-PEO metallo-supramolecular block copolymer containing a *bis*-terpyridine nickel (II) metal ligand complex located at the junction between the PS and PEO blocks. After self-assembly of this block copolymer in a thin film with an array of PEO cylinders oriented perpendicularly to the films surface, the PEO blocks have been extracted by washing with a methanol solution containing a competing ligand for terpyridine (CN^-).

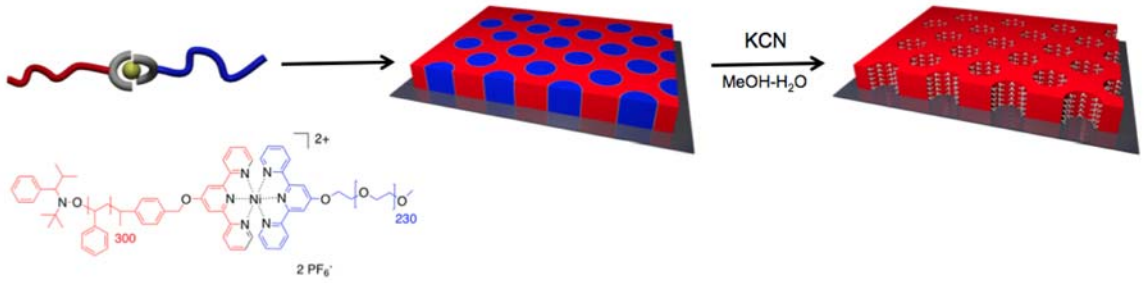

Figure 7.3: *Strategy towards nanoporous thin films form metallo-supramolecular block copolymers and chemical structure of the investigated block copolymer.*

This leaves a PS membrane functionalized by free terpyridine ligands on the pore walls. The availability of those terpyridine ligands has been proven by complexing them with Eu(III) ions, leading to fluorescent terpyridine Eu(III) complexes.

7.2. Post-functionalized pH and thermo-responsive asymmetric membranes

Integral asymmetric membranes prepared from polystyrene-*block*-poly(4-vinyl pyridine) (PS-P4VP) diblock copolymers have been post-functionalized. Those membranes are bearing 4-vinyl pyridine (4VP) units on the pore walls, which can be advantageously used for interactions through hydrogen bonding with H-donor containing molecules. In this respect, several small organic aromatic molecules bearing on one hand an H-donor group (carboxylic acid or hydroxyl group) and on the other hand another functional group (e.g. an aldehyde group prone for further reaction with an amine-containing molecule through imine bond formation) have been tested by HZG as post-functionalization agents for the PS-P4VP-based membranes. However, this post-functionalization strategy was not efficient. Therefore, molecules and polymers have been covalently grafted molecules on the pore walls. This has been achieved in two steps (Fig. 7.4). Firstly, the PS-P4VP membranes have been coated with *in-situ* formed polydopamine. In a second step, direct reaction of amine-functionalized molecules with the catechol motif of polydopamine through Michael nucleophilic addition was performed. This reaction proved to be highly efficient and was used for e.g. for the grafting of Jeffamine (a commercially available amino functionalized poly(ethylene glycol)) to the polydopamine-functionalized asymmetric membranes. Poly(*N*-isopropylacrylamide) (pNIPAM) has been also grafted on those membranes. This allows to obtain asymmetric membranes responding to pH (due to P4VP) and to temperature (due to pNIPAM) (Fig. 7.4). Water flux measurements show indeed a dramatic increase of the water flux above the lower critical solubility temperature of pNIPAM due to the collapse of these blocks on the pore walls.

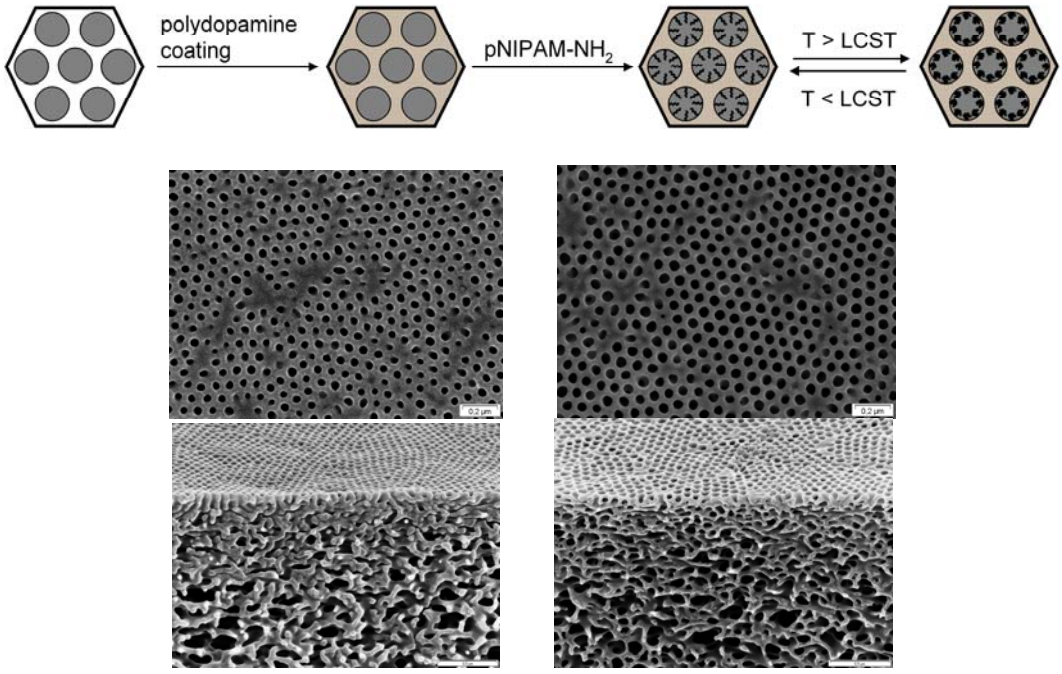

Figure 7.4: *Formation of pH and temperature-responsive membranes from pNIPAM-functionalized asymmetric polydopamine-coated PS-P4VP membranes. A scheme showing the temperature-response is included on top while below are shown electron microscopy images of the top and the side of the initial polydopamine-coated (left) and pNIPAM-functionalized membranes (right).*

7.3. Silicon-based membranes functionalized by (reactive) polymers

The functionalization of Si membrane nanopores with aluminum oxide has been demonstrated by CSEM using molecular vapor deposition (MVD). This technique allowed us to achieve conformal coating of nanopores with amorphous metal oxide layers of controllable thickness and it has been used for fabricating composite membranes with adjustable pore size by aluminum oxide coating. For instance, initial pore sizes of 80 nm have been reduced to ~20 nm by this method.

SiN membranes have been also functionalized by CSEM by chemi- or physisorption of various molecules. Special interest was devoted to antifouling biocompatible PEO-based coatings for further biomedical applications of the membranes. Diblock copolymers of poly(L-lysine)-*block*-PEO have been first adsorbed on SiN surfaces through electrostatic interactions. No adsorption of labeled-bovine serum albumine (BSA) was detected on the poly(L-lysine)-*block*-PEO coated surface. The drawback of this approach is, however, a non-covalent grafting of the anti-fouling material on the membrane surface that could be affected by pH and ionic strength changes. In a second strategy, a trimethoxysilane terminated PEO has been used to create a chemically grafted self-assembled monolayer on the SiN surface. However, a low reduction of BSA adsorption was noted for the accordingly treated surface. This is thought to result from the too low molecular weight of the grafted PEO. The grafting of an amino-terminated poly(ethylene glycol) on an isocyanate-functionalized SiN surface has been realized by melt extrusion. The process was quite efficient. Protein adsorption is as much reduced as the length of the grafted PEO is high.

SiN membranes were also functionalized with amphoteric hydrogels. This work was conducted in collaboration with Rhenovia. A new generation of isoelectric focusing membranes for charge-based separation of proteins has been obtained. Briefly, silicon chips carrying 4x 100 nm thick SiN membranes were first functionalized with a silane terminated with reactive double bonds. Then, polyacrylamide-based hydrogels containing amphoteric monomers, called immobilines, were cast on the membrane surface in order to impose various pH values, 5.20, 5.30, 5.45 and 5.55, as shown in Fig. 7.5. The use of hydrogel-based silicon chips for charge-based protein separation was demonstrated by using an E-coli lysate, whose total protein fingerprint is shown in Fig. 7.5 (right, column 3). The two fractions collected between hydrogel-based SiN membranes having a difference of 0.1 pH unit are also shown on the same picture, thus demonstrating the proof of concept for the fractionation of complex protein samples by isoelectric focusing.

An Atom-Transfer Radical Polymerization (ATRP) initiator has been grafted by UCL on model Si and SiN wafers. In a second step, statistical copolymerization of N-acryloxysuccinimide (NAS) and oligo(ethylene methacrylate) (OEGMA) has been performed from the grafted initiator. The NAS group is an activated ester designed for further reaction with amine-containing molecules while OEGMA is a water-soluble thermoresponsive monomer allowing water-solubility of the polymer brush. Although, this copolymerization encountered a problem of reactivity (NAS is too reactive compared to OEGMA), starving polymerization conditions (controlled addition of a small amount of NAS at the end of the polymerization) allowed the formation of the desired water-soluble reactive polymer brushes. Polymer brushes with thicknesses of ca. 30 nm have been obtained either on Si or SiN wafers, as measured by ellipsometry. The reactivity of NAS moieties has been finally checked by grafting a fluorescent dye.

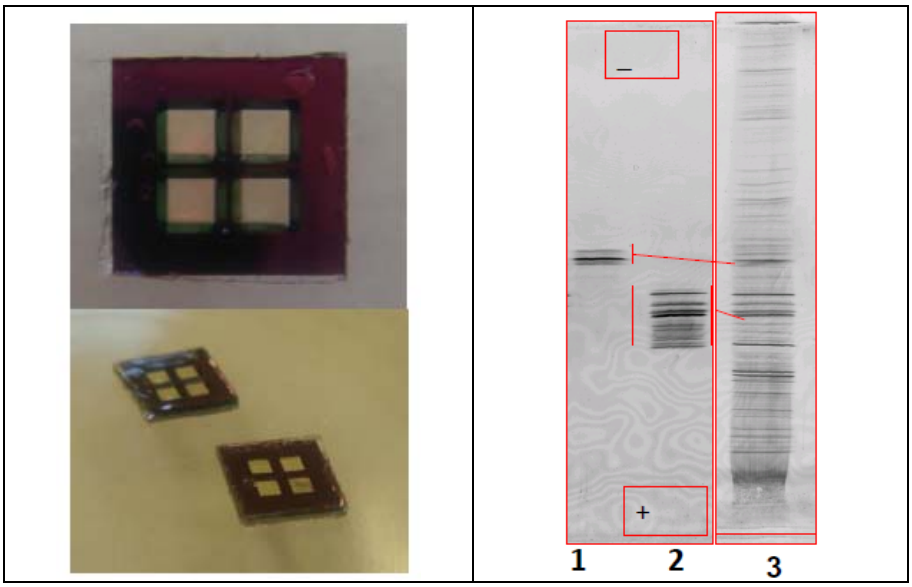

Figure 7.5: *(left) silicon chips carrying 4x 100 nm thick SiN membranes functionalized with IEF hydrogel. (right) column 1: protein fraction recovered between PH 5.45-5.55, column 2: protein fraction recovered between pH 5.20-5.30, column 3: E-coli lysate in a Rabilloud buffer. Dry IPG pH 4-7.*

Work Package 8: Evaluation of Membranes for Gas Separation, Biomolecule Separations and Medical Water Applications

The objective of this work package was to evaluate the permeability and selectivity of membranes that have been fabricated using polymer self-assembly. By utilising polymer-based and silicon-based membranes formed as part of work packages 5, 6 and 7 we aimed to study 4 industrially relevant application areas:

- Gas separations
- Medical water filtration
- Protein separations
- Affinity chromatography

Evaluation of membranes was conducted at Helmholtz-Zentrum Geesthacht (HZG), Centre Suisse d'Electronique et de Microtechnique (CSEM), Air Liquide (AL), Rhenovia Pharma (RHE) and Pall Europe Ltd (PEL), with additional analytical support being provided by Technion (TECH). To facilitate testing in these application areas, key performance indicators were set and used for the iterative development of membranes.

1. Polymeric Membranes

A number of polymeric membranes were provided throughout the project by work packages 5 and 7 that were evaluated against the application targets detailed below. Initial membrane samples that were cast on poly(acrylonitrile) were found to be non-porous despite possessing a well defined self-assembled surface, prompting a change of support to a non-woven material. This resulted in further development work being required, yielding final membranes that possessed porous hexagonally packed self-assembled structures.

SEM analysis of the membrane surface revealed that the majority of these membranes had pore diameters within the target range for medical water filtration and protein separation applications (50-100 nm), with those remaining having smaller pores. Shown below are the results of the membrane analysis when compared to the application areas detailed above.

1.1 Medical Water Filtration

Key performance indicators: 50-100 nm pore size, absolute sterilization, and at least 1000 L m^{-2} h^{-1} at < 1 bar pressure.

Water flow measurements showed that the majority of tested membranes possessed an initial water flow greater than the target of 1000 $Lm^{-2}hr^{-1}$ at <1 bar pressure, though flow rates were observed to decrease over time due to a combination of pore swelling and fouling. Bacterial challenge experiments revealed that bacteria passed through all tested samples, probably due to cracks that formed through the thin retentive layer of the surface (Fig. 8.1).

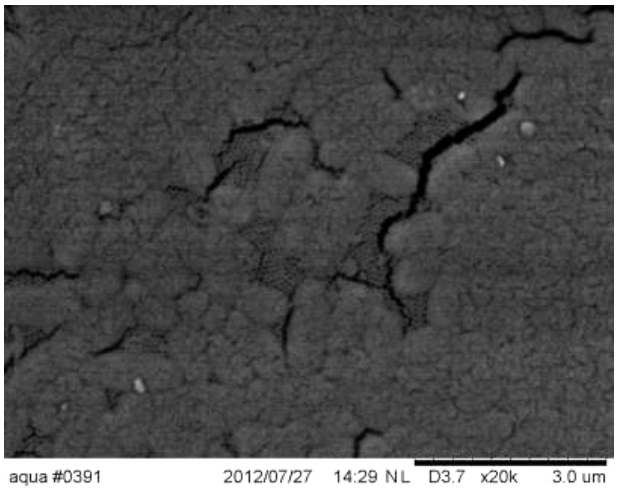

Figure 8.1: *SEM image taken of a membrane after bacterial challenge revealing cracks on its' surface.*

1.2 Protein Separations

Key performance indicators: 50-100 nm pore size, fractionation of test proteins 10-150 KDa by crossflow with an average flux rate of 30 L m^{-2} h^{-1} at 2 bar trans membrane pressure.

Protein retention experiments were undertaken using two proteins of differing molecular weight, BSA (67 kDa) and IgG (150 kDa), and showed that the percentage retention of IgG is far greater than that of BSA, with flow rates that are above the required target. It was observed that there was no direct correlation between percentage retention and pore size, suggesting that other interactions may be occurring.

1.3 Affinity Chromatography

Key performance indicators: 100 nm pore size required. Aldehyde, carboxyl, primary amine or epoxy functionalities on membranes. Use immobilized Protein A to give at least 50 mg/ml IgG/ml membrane volume capacity at 5-10 MV/min and < 1 bar pressure.

Work to study the affinity chromatographic properties were hampered by the reaction conditions and chemistries involved in the functionlisation and modification of the PS-*b*-4VP

membranes which resulted in damage to the membrane surface. As a final attempt, samples of membrane were formed *via* spin-coating of a poly(styrene)-poly(ethylene oxide) block copolymer bearing a photo-cleavable group onto non-woven and functionalised with Protein A. However, no binding of IgG was observed, possibly as a result of too little ligand density or too high a flow rate of IgG solution.

2 Inorganic Membranes

2.1 Nanofabrication and Membrane Specifications

The nanoporous silicon nitride membranes (NSiMs) used in this study are shown in Fig. 6.2. They exhibit a mean pore diameter of 95 nm and a density of ~4 x 10^9 pores/cm^2, corresponding to a void fraction of about 0.2.

2.2 Molecular Transport and Size-based Filtration through Nanopores

The interest of high flux membranes like NSiMs relies on the fact that they are able to perform molecular filtration at lower pressures, with reduced filtration times, and thus at lower operational costs.

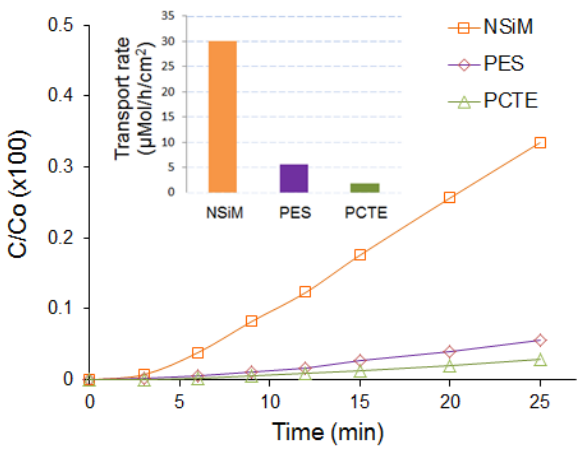

Figure 8.2: *Diffusion of fluorescein through NSiM (pore size: 95 nm) and comparison against two commercial polymeric membranes: PES (Sartorius, pore size: 100 nm) and PCTE (Whatman, pore size: 200 nm). The insert shows the value of the flux determined for the three membranes.*

Permeation experiments were carried out using home-made polycarbonate fluidic cells. Transport rates of fluorescein (a low MW dye molecule) through NSiMs were measured and the results compared against commercial PCTE and PES ultrafiltration membranes of similar pore sizes. The results (Fig. 8.2) show that the transport rate of fluorescein is fastest through the NSiM; it is 5 times and 16 times faster than that of the commercial PES and PCTE, respectively.

A second series of experiments was conducted using FITC-labeled dextrans of various MWs (150, 500 and 2000 kDa) that demonstrated the ability of NSiMs to achieve size-based filtration.
As expected, the transport rates were highly dependent on dextran MWs with the shorter dextran diffusing rapidly and the longer dextran being almost completely hindered. From the observed diffusion rates, we can estimate selectivities of ~6 between dextrans 150 KDa/500 kDa and ~50 between dextrans 150 KDa/2000 kDa. As the observed selectivity ratios are much higher than the differences of diffusion coefficients for the three dextrans, we have an effective filtration based on molecular sizes.

2.3 Affinity-based Separation within Nanopores

The ability to capture and detect analyte biomolecules, such as proteins, enzymes or nucleic acids, with a high selectivity and sensitivity is of great importance in pharmaceutical and diagnostic applications. Here, we have demonstrated the potential of silicon-based membranes produced in SELFMEM for conducting biomolecular reactions inside pores. The concept was demonstrated using microporous silicon nitride membranes (MSiMs), which are 500 nm free-standing SiN membranes composed of isodisperse pores of about 1.5 micron in diameter.
After immobilizing biotin on the membrane using dextran-based polysaccharides, the chips were treated with Cy5-streptavidin and any resulting fluorescence recorded (Fig. 8.3). Whereas no fluorescence signal is observed for the chip coated only with dextran-biotin, the 9 membranes after treatment show a high fluorescence signal (16000 a.u.) which attest of the binding of Cy5-strepavidin inside the pores. The difference in fluorescence intensity of the membrane surface (green) and the plain silicon frame (blue) for the dextran-biotin + Cy5-streptavidin system allows us to estimate a signal increase of about 6 fold on the porous area which may be assigned to the confinement effect within the pore, thus improving the efficiency that an analyte transfers from a liquid phase to the stationary phase.

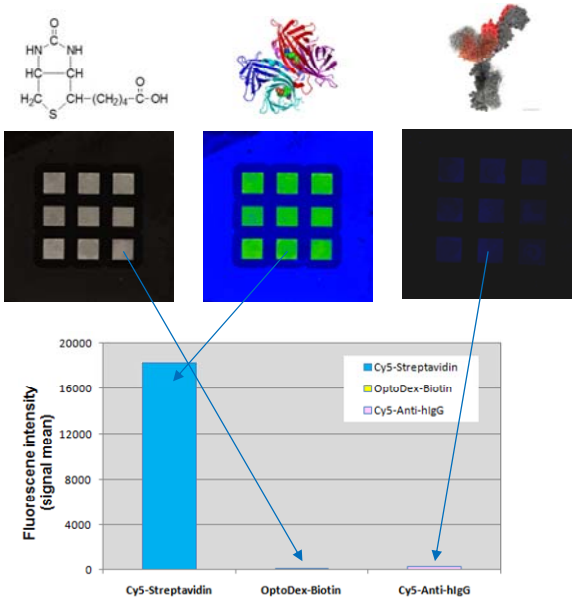

Figure 8.3: *Silicon chips carrying an array of 3 x 3 MSiMs functionalized with (left) dextran-biotin, (middle) dextran-biotin + Cy5-streptavidin, and (right) dextran-biotin + Cy5- Anti-hIgG.*